UCLA
UCLA Previously Published Works

Title

Amplitude Dependence of Nonlinear Precipitation Blocking of Relativistic Electrons by Large Amplitude EMIC Waves

Permalink

https://escholarship.org/uc/item/19w655h6

Journal

Geophysical Research Letters, 49(12)

ISSN

0094-8276

Authors

Bortnik, Jacob
Albert, Jay M
Artemyev, Anton
et al.

Publication Date

2022-06-28

DOI

10.1029/2022gl098365

Peer reviewed

Geophysical Research Letters®

Key Points:

- The range of nonlinear responses of energetic electrons interacting with intense ElectroMagnetic Ion Cyclotron (EMIC) waves is studied using a test-particle code
- Resonant energetic electrons at low pitch angles experience nonlinear force bunching which rapidly advects them to large pitch angles
- Increasing EMIC wave amplitudes enhances the force bunching positive advection relative to diffusion resulting in precipitation blocking

Correspondence to:

J. Bortnik,
jbortnik@ucla.edu

Amplitude Dependence of Nonlinear Precipitation Blocking of Relativistic Electrons by Large Amplitude EMIC Waves

Jacob Bortnik[1] [ID]**, Jay M. Albert[2]** [ID]**, Anton Artemyev[3,4]** [ID]**, Wen Li[5]** [ID]**, Chae-Woo Jun[6]** [ID]**, Veronika S. Grach[7]** [ID]**, and Andrei G. Demekhov[7,8]** [ID]

[1]Department of Atmospheric and Oceanic Sciences, University of California at Los Angeles, Los Angeles, CA, USA, [2]United States Air Force Research Laboratory, Albuquerque, NM, USA, [3]Department of Earth, Planetary, and Space Sciences, University of California at Los Angeles, Los Angeles, CA, USA, [4]Space Research Institute RAS, Moscow, Russia, [5]Center for Space Physics, Boston University, Boston, MA, USA, [6]Solar-Terrestrial Environment Laboratory, Nagoya-Shi, Japan, [7]Institute of Applied Physics, Russian Academy of Sciences, Nizhny Novgorod, Russia, [8]Polar Geophysical Institute, Apatity, Russia

Abstract Recent work has shown that ElectroMagnetic Ion Cyclotron (EMIC) waves tend to occur in four distinct regions, each having their own characteristics and morphology. Here, we use nonlinear test-particle simulations to examine the range of energetic electron scattering responses to two EMIC wave groups that occur at low L-shells and overlap the outer radiation belt electrons. The first group consists of low-density, H-band region b waves, and the second group consists of high-density, He-band region c waves. Results show that while low-density EMIC waves cannot precipitate electrons below ∼16 MeV, the high density EMIC waves drive a range of linear and nonlinear behaviors including phase bunching and trapping. In particular, a nonlinear force bunching effect can rapidly advect electrons at low pitch-angles near the minimum resonant energy to larger pitch angles, effectively blocking precipitation and loss. This effect contradicts conventional expectations and may have profound implication for observational campaigns.

Plain Language Summary Based on a recent study that has shown how ElectroMagnetic Ion Cyclotron (EMIC) waves tend to occur in four distinct regions, we study two of those regions that occur at relatively low L-shells, and overlap with the intense portion of the outer radiation belt energetic electrons. We use a nonlinear, test particle code to simulate the wave-particle interaction of energetic electrons with two groups of waves: high-density, He-band EMIC waves and low-density, H-band EMIC waves. While the low-density EMIC waves have resonant energies that are too high to affect the typical range of radiation belt electrons, the high-density EMIC waves drive a range of linear and nonlinear responses in the electrons. In particular, as the EMIC waves get more intense, a nonlinear "force bunching" effect tends to reflect energetic electrons at low pitch angles out of the loss cone, and prevent them from precipitating, contrary to expectations based on quasilinear and (more conventional) nonlinear theory. The precipitation blocking could have profound effects on observational campaigns that attempt to simultaneously measure EMIC waves near the geomagnetic equator, and result in coincident precipitation along the same field line at low altitudes, in that the precipitation could be entirely absent.

1. Introduction

ElectroMagnetic Ion Cyclotron (EMIC) waves are a class of naturally-occurring plasma emissions that are found ubiquitously in the Earth's magnetosphere, having frequencies in the Pc1-Pc2 (∼0.1–5 Hz) range, and are typically excited in the L-mode near the geomagnetic equator in association with intensified geomagnetic activity (Jordanova et al., 2006; Loto'aniu et al., 2005). The free energy source driving the excitation of EMIC waves is thought to be the thermal anisotropy of the energetic (tens of keV) protons (Anderson et al., 1996; Kennel & Petschek, 1966; Horne & Thorne, 1993; Mauk & Mcpherron, 1980; Rauch & Roux, 1982; Young et al., 1981), and the presence of heavy ions further divides the EMIC spectrum into frequency bands that are labeled according to the ion gyrofrequency below which the band is found, for example, H^+-, He^+-, and O^+-band EMIC waves occur directly below the H^+-, He^+-, and O^+-gyrofrequencies (f_{cH}, f_{cHe}, and f_{cO}) (Gomberoff & Neira, 1983; Horne & Thorne, 1994; Kozyra et al., 1984; Young et al., 1981).

Although the spatial distribution of EMIC waves and their associated characteristics have been studied for a number of years (Anderson et al., 1992a, 1992b; Halford et al., 2010; Kasahara et al., 1992; Keika et al., 2013;
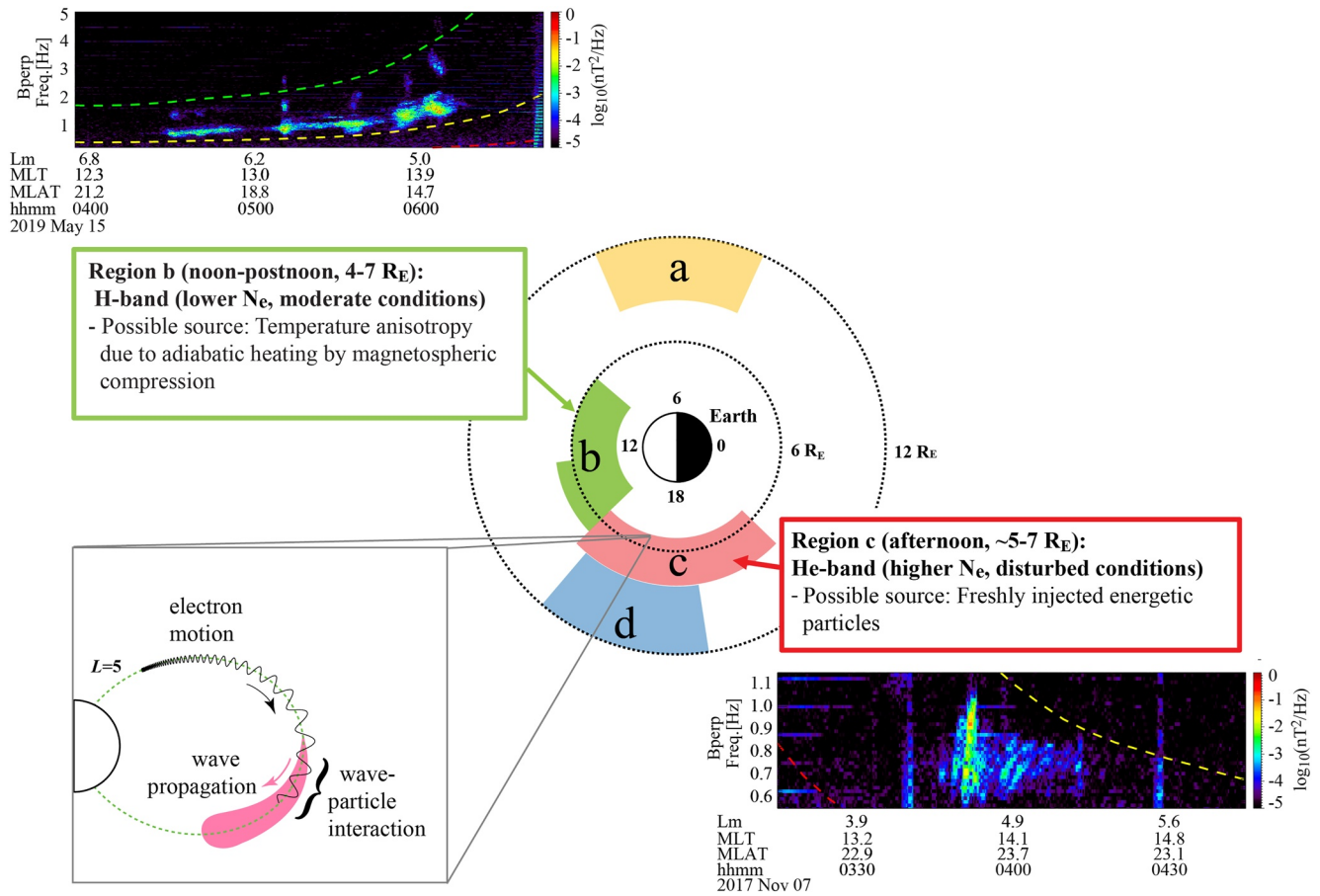
Figure 1. Graphical illustration of the four primary EMIC wave regions a-d based on Figure 11 of Jun et al. (2021). Top left: Region b EMIC wave characteristics with an illustrative example of H-band waves observed on the Arase satellite on 15 May 2019. Bottom right: Region c EMIC wave characteristics with an illustrative example of He-band waves from the Arase satellite on 7 Nov 2017. Bottom left: a schematic showing the wave-particle interaction geometry, with the energetic electron propagating through the EMIC wave packet, both heading toward the South.

Meredith et al., 2014; Min et al., 2012; Saikin et al., 2015; Usanova et al., 2012, 2013), the recent availability of high-resolution, long-term, multi-spacecraft, full-spatial coverage datasets has allowed an unprecedented level of detail to be achieved in such observations. For example, using a combined dataset of Van Allen Probes (Mauk et al., 2013) and Arase (Miyoshi et al., 2018) observations, Jun et al. (2021) demonstrated that EMIC waves tend to naturally group into four distinct occurrence regions, each with its own unique morphology and driving conditions, shown in the central panel of Figure 1, labeled a-d.

While the high L-shell (>8 R_E) regions (a and d) are associated with weaker wave amplitudes and quiet to moderate geomagnetic conditions, it is the low L-shell (<6 R_E) regions (b and c) identified in Jun et al. (2021) that are of primary interest to the present study, due to their relatively large intensities, association with geomagnetically active conditions, and—very importantly—their spatial overlap with the high-energy, outer electron radiation belt electron population (typically spanning L ~ 3–6, with peak fluxes at L ~ 4–5).

Region b is characterized by H^+-band EMIC waves occurring on the dayside, in the low-density region outside the plasmasphere, over the region L ~ 3–6 and observed during the recovery phase of geomagnetic storms, often in association with moderate substorms and solar wind pressure enhancements. These waves are predominantly left-hand polarized, with center frequencies in the range of 0.7–4.0 Hz.

In contrast, region c is characterized by He^+-band EMIC waves occurring on the duskside, high-density region inside the plasmasphere, over the region L ~ 5–7, during the main phase of geomagnetic storms. Typical examples of both types of EMIC waves are shown in the breakout panels in Figure 1, as observed by the Arase satellite, where the green, yellow, and red dashed lines in both spectrograms correspond to f_{cH}, f_{cHe}, and f_{cO}.

The average EMIC wave intensities in both regions b and c are on the order of ~1 nT, which is consistent with previous studies reporting EMIC amplitudes in the range of ~1–10 nT, and higher (Engebretson et al., 2015; Fraser et al., 2010; Meredith et al., 2003). Such intense EMIC waves inevitably drive strong scattering of energetic electrons, and numerous studies employing a quasilinear diffusive framework have shown that EMIC waves with amplitudes of ~1 nT (particularly in conjunction with whistler mode chorus and hiss waves) can drive precipitation near the strong diffusion limit (i.e., where electrons are scattered into the loss cone faster than they can be removed through precipitation to the atmosphere) (Shprits et al., 2009) and act as a rapid loss mechanism for outer radiation belt electrons of energies >1 MeV on the timescale of a day (e.g., Albert, 2003; Jordanova et al., 2008; Li & Hudson, 2019; Miyoshi et al., 2008; Shprits et al., 2016, 2017; Summers & Thorne, 2003; Thorne & Kennel, 1971; Thorne et al., 2005, 2006).

However, the large EMIC wave amplitudes naturally call into question the validity of the quasilinear diffusive framework, and a number of recent studies have demonstrated a range of nonlinear effects including the familiar phase bunching and trapping (e.g., Albert & Bortnik, 2009; Liu et al., 2012; Omura & Zhao, 2012), non-resonant scattering (Chen et al., 2016), and a somewhat less-discussed nonlinear effect called force bunching, originally studied in the context of electron interactions with whistler-mode waves (Inan et al., 1978, p. 3241; Lundin & Shklyar, 1977), and more recently in the context of EMIC waves (Grach & Demekhov, 2020).

The present study aims to contrast the range of nonlinear effects induced by EMIC waves corresponding to regions b and c (Figure 1) as a function of electron energy and pitch angle, and to specifically focus on the effects of force bunching as a function of wave amplitude in potentially preventing electron precipitation at low pitch-angles (i.e., precipitation blocking). Section 2 presents the test-particle methodology and Section 3 describes the results, before the discussion and summary sections conclude this report.

2. Methodology

In order to quantify the nonlinear scattering effects of EMIC waves on energetic electrons, the full set of gyroresonance-averaged equations of motions is followed for a group of 12 electrons, uniformly distributed in initial gyrophase, originating from the equator and traveling in a southward direction through the EMIC wave packet, as illustrated graphically in the bottom-left panel of Figure 1. These nonlinear wave-particle equations are adapted from previous whistler-mode studies (e.g., Bortnik et al., 2006; Bortnik & Thorne, 2010) by using the L-mode branch of the plasma dispersion relation, and assuming field-aligned waves, resulting in a set of equations that is identical to Albert and Bortnik (2009), written as:

$$\frac{dp_\parallel}{dt} = eB_w \frac{p_\perp}{m\gamma} \sin\eta - \frac{p_\perp^2}{2m\gamma B} \frac{\partial B}{\partial z} \tag{1}$$

$$\frac{dp_\perp}{dt} = eB_w \left(\frac{\omega}{k} - \frac{p_\parallel}{m\gamma} \right) \sin\eta + \frac{p_\perp p_\parallel}{2m\gamma B} \frac{\partial B}{\partial z} \tag{2}$$

$$\frac{d\eta}{dt} = \left(\frac{kp_\parallel}{m\gamma} - \omega - \frac{\Omega}{\gamma} \right) + eB_w \left(\frac{\omega}{k} - \frac{p_\parallel}{m\gamma} \right) \frac{\cos\eta}{p_\perp} \tag{3}$$

$$\frac{d\lambda}{dt} = \frac{p_\parallel}{m\gamma} \frac{1}{L R_E \cos\lambda \sqrt{1 + 3\sin^2\lambda}} \tag{4}$$

Here $p_\perp, p_\parallel$ are the components of the electron momentum ($p = \gamma mv = mv/\sqrt{1 - v^2/c^2}$) perpendicular and parallel to the background magnetic field B (having associated electron gyrofrequency $\Omega = eB/m$), the EMIC wave intensity is represented by the perpendicular component of the wave magnetic field B_w, and the wave radial frequency and wave number are given by ω, k which are related by the multi-species, cold-plasma dispersion relationship. The wave-particle phase η is the angle between the vectors $-B_w$ and $p_\perp$ and resonance is typically identified when this phase is quasi-stationary, that is, $\frac{d\eta}{dt} = 0$. The particles' latitudinal position (λ) at a particular L-shell (L) is described by 4, where $R_E = 6370$ km is the Earth's assumed radius, and z represents the distance measured from the equator along the magnetic field line.

In the following simulations, we focus on the $L = 5$ field line (corresponding to $f_{cH} = 3.83$ Hz at the equator, with a dipolar latitudinal variation) since it represents the location where both region b and c EMIC waves are present, and overlaps with the heart of the outer radiation belt. Focusing on a common L-shell allows us to make a fair comparison between the effects of region b and c EMIC waves without the added variation of the magnetic field intensity. While a dipolar magnetic field model has been historically used in test-particle simulations (e.g., Albert & Bortnik, 2009; Artemyev et al., 2021; Grach et al., 2021; Inan et al., 1978; Lundin & Shklyar, 1977 and references therein) and is typically a good representation of the real magnetic field in the inner magnetosphere, it should nevertheless be noted that during intense storms, even the $L \sim 5$ region can become somewhat stretched and deviate from a strictly dipolar variation (e.g., Rae et al., 2019, Figure 3a). This field stretching is beyond the scope of the current study, but its effects should be examined in future work.

The electron density model is described by the equation $n_e = n_{e0}\cos^{-2s}\lambda$ (Denton et al., 2002), with the values $n_{e0} = 7$ el/cc and $n_{e0} = 220$ el/cc adopted for regions b and c, respectively, following typical plasma trough and plasmasphere densities at $L = 5$ (Carpenter & Anderson, 1992) with corresponding index values of $s = 1$ and $s = 0.5$ (Denton et al., 2002). The ion concentration is assumed to be constant with latitude, with the commonly used ratios $n_H/n_e = 0.77$, $n_{He}/n_e = 0.2$, and $n_O/n_e = 0.03$ (Albert & Bortnik, 2009; Jordanova et al., 2008). The wave frequencies adopted for regions b and c were $f_b = 1.9$ Hz and $f_c = 0.77$ Hz corresponding to typical H-band and He-band wave frequencies at $L = 5$, respectively (Jun et al., 2021), with a field-aligned wave normal angle. The latitudinal amplitude variation was taken similar to Bortnik et al. (2008), that is, increasing smoothly in the equatorial region to its maximum value B_w^0 over the span of a few degrees, and is given by $B_w = B_w^0[\tanh(-\lambda - 2) + 1]/2$. This smooth variation prevents any artificial discontinuities in the wave amplitude and any resultant particle scattering due to such discontinuities.

3. Results

A few representative particle trajectories are shown in Figure 2, with initial (equatorial) conditions listed in the figure title, showing the (equatorially mapped) pitch-angle variation as a function of particle latitude, propagating from right to left in the figures. Figure 2a shows the trajectories of non-resonant electrons, where the pitch angle of each particle temporarily oscillates as it traverses the EMIC wave packet, but is not permanently altered leading to no permanent scattering over the set of particles. Figure 2b shows the particle trajectories of electrons experiencing a "quasi-linear" interaction, namely pitch angles that are scattered symmetrically to larger and smaller pitch angles, with a roughly zero mean, and sinusoidal pitch angle change as a function of initial wave-particle phase. Such interactions can form the basis of quasilinear diffusion, when they are of small amplitude, experienced successively, with a large number of phase uncorrelated wave packets (the details of the relationship between individual EMIC wave-particle interactions and how they could lead to quasilinear diffusion are nuanced and discussed in detail in, e.g., Zheng et al., 2019). Figure 2c shows the effects of force bunching which result from the second term in 3 becoming dominant when pitch angles become small and $p_\perp \to 0$ (analogous to the whistler case, examined by, e.g., Albert et al., 2021; Artemyev et al., 2021; Inan et al., 1978; Kitahara & Katoh, 2019; Lundin & Shklyar, 1977). Under such conditions, the wave-particle phases become bunched, and a rapid advection displaces all the particle pitch angles approximately uniformly to much larger values, where there are stably trapped (as opposed to their initial "precipitating" state). The final example in Figure 2d shows the effects of nonlinear phase-trapping (e.g., Albert & Bortnik, 2009; Grach & Demekhov, 2018a) which results from trapping the electron in the wave potential, and forcing the electron parallel velocity to follow the resonant velocity along its trajectory. This interaction results in a rapid advection of medium to high pitch angle particles to much lower values, in the present example by as much as $\Delta\alpha = 45°$.

In order to examine the full range of particle scattering effects, we show a summary of the scattering characteristics of region c (high-density) EMIC waves in Figure 3, where each of the panels shows a scattering property (using the color axis) as a function of initial pitch-angle (abscissa) and energy (ordinate), parameterized by the assumed EMIC wave intensity corresponding to each of the rows. The columns represent the mean pitch angle change (left column) of each group of test-particles, as depicted in Figure 2c and shown in red font, and the standard deviation of the pitch angle change (middle column) of the group of particles as indicated by the blue font in Figure 2c, which can be crudely thought to represent the advective and diffusive portions of the scattering process, respectively. The rightmost column shows the ratio of the mean to the standard deviation (i.e., an
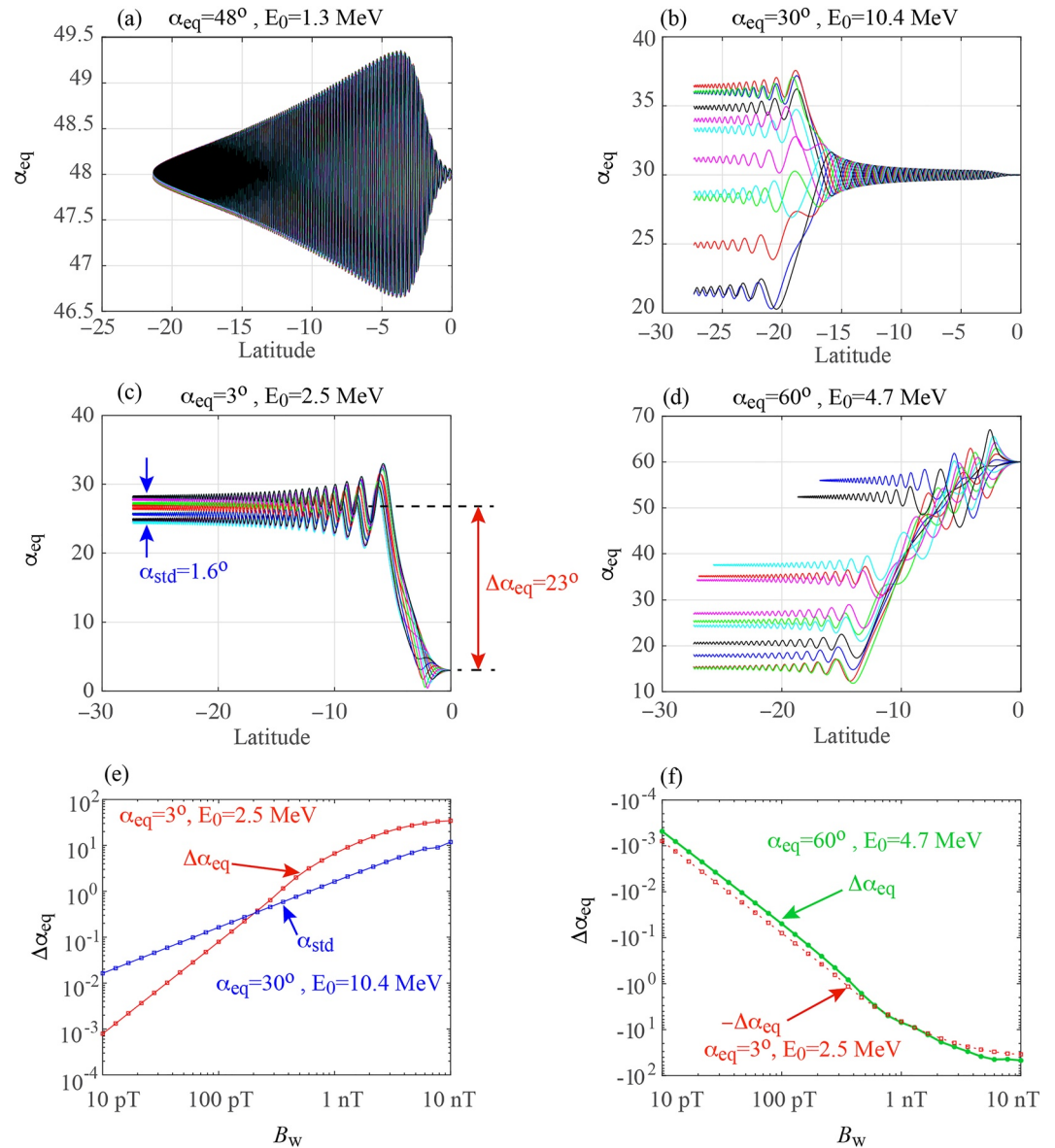
Figure 2. An illustration of four typical energetic electron pitch-angle trajectories in the high-density Region c, with 12 particles shown for each case, distributed uniformly in initial gyrophase. (a) Non-resonant scattering, (b) Resonant quasilinear scattering, (c) Strong positive advection due to force bunching, and (d) Strong negative advection due to phase trapping. (e) EMIC wave amplitude dependence of the near loss-cone electron advection (red) compared to the standard deviation of the pitch angle for resonantly scattered electrons (blue). (f) Similar to (e) but showing the negatively advecting electrons (green), compared to the (absolute value) of the positively advected near loss-cone electrons (red dotted). The specific initial electron pitch angle and energy values are shown in each panel, and the EMIC wave amplitude is 3.6 nT in (a)–(d).

element-wise division of the left, by the middle column values), which can serve as an indicator of where nonlinear advective scattering becomes important relative to diffusive scattering. It should be noted that here "diffusive" scattering is used in a crude sense and essentially represents symmetrical scattering with minimal change in the mean pitch angle, whereas truly diffusive scattering can only be confirmed by examining the distribution of pitch angle changes of all the particles.

Examining the middle (standard deviation) column, it is apparent that a minimum resonant energy exists at E ~ 2.5 MeV when $p_\perp = 0$, below which only non-resonant interactions take place (e.g., Figure 2a) which do not produce any significant change in the standard deviation. Significant scattering abruptly begins the when the particle parallel energy exceeds the minimum resonant energy, and slowly decreases as the energy is further
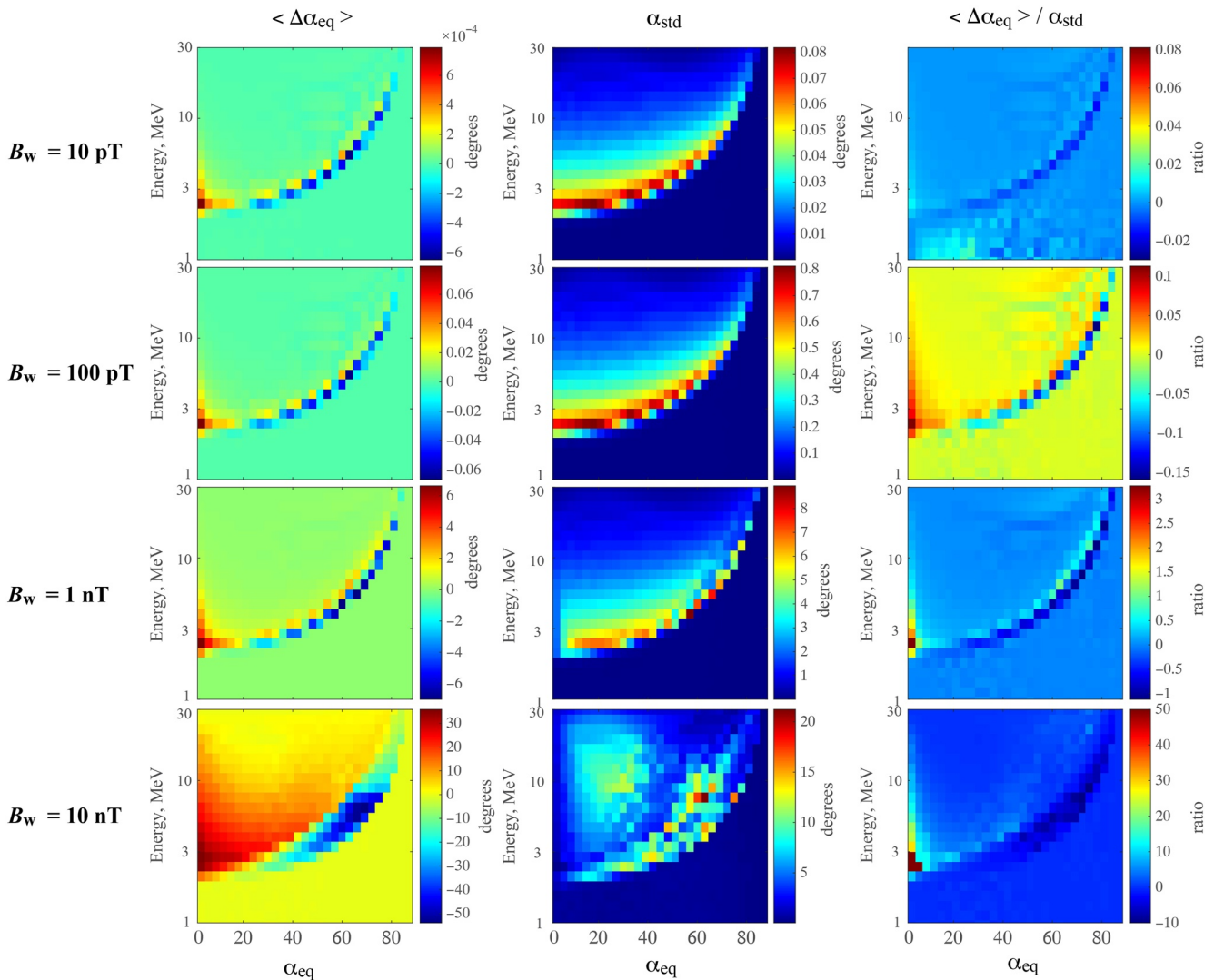
Figure 3. Scattering characteristics corresponding to the high-density Region c. Single-pass, phase-averaged scattering characteristics of a group of 12 energetic electrons passing through a He-band EMIC wave field, shown as a function of initial electron pitch angle on the abscissa (α_{eq}) and initial electron energy in MeV on the ordinate. The rows are parameterized by EMIC wave amplitude (top to bottom: 10 pT, 100 pT, 1 nT, and 10 nT) and columns correspond to (left) mean pitch angle change $<\Delta\alpha_{eq}>$, (middle) standard deviation of pitch angle change $<\left(\Delta\alpha_{eq} - <\Delta\alpha_{eq}>\right)^2>^{1/2}$, and (right) mean divided by standard deviation. Note the changing color scales in each panel.

increased, since the wave-particle resonant location moves to higher latitudes. At larger pitch-angles, the resonant energy increases consistently with the standard single wave characteristic (Walker, 1993).

The mean pitch angle deviation (left-most column) shows that even at the lowest EMIC wave intensity (10 pT, top row), there is a pronounced positive advection at the minimum resonant energy when $p_\perp = 0$, due to nonlinear force bunching (e.g., Figure 2c) but at larger pitch angles this advective motion becomes negative (blue color), and transports particles to lower pitch angles due to phase trapping (e.g., Figure 2d). However, a comparison of the advective and diffuse scattering terms (right-most column) shows that for the weakest waves, the mean advective motion represents only a small fraction (few percent) of the standard deviation of the scattering, indicating that particle scattering is essentially diffusive.

As the EMIC wave intensity is increased from 100 pT (second row) to 10 nT (bottom row), the $\alpha - E$ region affected by strong advection increases in size and intensity, often reaching pitch angle advection values of $\Delta\alpha > 30°$, such that the advective terms begin to dominate over the diffusive terms. In particular, the group of particles at the minimum resonant energy ($\alpha = 0$) can experience advective motion to larger pitch angles which

can exceed the diffusive spreading by a factor of 50 (bottom, right column), effectively "blocking" the precipitation of these particles into the atmospheric loss cone.

In order to study the amplitude dependence of the force bunching effect, we show in Figure 2e the mean pitch angle change ($\Delta\alpha_{eq}$) of the minimum resonant energy electrons (shown in red, similar to Figure 2c, with $\alpha_{eq} = 3°$, $E_0 = 2.5\,\text{MeV}$), and compare it to the standard deviation of the diffusively scattered electrons (shown in blue, similar to Figure 2d, $\alpha_{eq} = 30°$, $E_0 = 10.4\,\text{MeV}$) as a function of EMIC wave intensity. Immediately apparent is that the advective term is significantly weaker (more than an order of magnitude) than the diffusive term at low EMIC wave intensities (10 pT) and can be considered to be in the linear scattering regime. This advective term increases rapidly, roughly $\Delta\alpha_{eq} \propto B_w^2$ whereas the diffusive term increases slower, roughly $\alpha_{std} \propto B_w$ such that at ~200 pT the two terms become comparable. At ~1 nT the advective term dominates over the diffusive term and the interaction can be considered to be in the nonlinear regime. It is also important to note that beyond this point, the amplitude dependence of the force bunching term changes and becomes closer to $\Delta\alpha_{eq} \propto B_w^{1/2}$.

Interestingly, a comparison of the amplitude dependence of the two dominant nonlinear advection effects, namely force bunching and phase trapping (e.g., bottom left panel of Figure 3) shown in Figure 2f reveals that these two effects not only have nearly identical absolute values, but indeed scale as a function of wave amplitude in almost the same way. Perhaps not surprisingly, over the 'long term' (i.e., many successive wave-particle interactions), these nonlinear effects can compensate for one another, and the overall particle scattering could again appear to be diffusive, though proceeding on timescales much faster than those of quasilinear diffusion (e.g., Omura & Zhao, 2013; Grach & Demekhov, 2020; Kubota & Omura, 2017).

Figure 4 shows a summary of the scattering results in the same format as Figure 3, but with wave characteristics and background parameters set to represent the low-density, H-band, region c (Figure 1) EMIC waves, as described in Section 2 above. While the major features and scattering regions in Figure 4 are similar to those in Figure 3, a notable difference is that the minimum resonance energy of electrons now exceeds 16 MeV, which makes region b waves relatively ineffective for scattering the bulk of the radiation belt electrons which typically span energies of ~0.5 MeV to several MeV. The force bunching effect is still evident and dominates over the diffusive scattering near the minimum resonant energy at large EMIC wave amplitudes (B_w ~10 nT) but with factors of ~10–15, that is, to a far lesser degree than the high-density region c waves.

4. Discussion

The results presented in Figures 2–4 suggest that for the case of a single-pass interaction considered in the present study, that is, when energetic electrons with pitch angles close to the atmospheric bounce loss-cone stream through an EMIC wave packet, they would not necessarily be precipitated and lost into the dense upper atmosphere as would be expected on the basis of the often-used quasilinear theory (e.g., Jordanova et al., 2008; Li & Hudson, 2019; Miyoshi et al., 2008; Shprits et al., 2016, 2017; Summers & Thorne, 2003; Thorne & Kennel, 1971; Thorne et al., 2005, 2006). Indeed, for moderate to intense EMIC wave packets, such resonant electrons would be rapidly (i.e., on the order of tens of milliseconds) advected to large pitch angles within the course of a single wave-particle interaction, and effectively be "blocked" from precipitating. As such, coordinated observations between in situ spacecraft that aim to observe the driving EMIC waves near the equatorial region of a given field line, and Low-Earth Orbiting spacecraft that attempt to observe the resultant energetic electron precipitation at the footpoint of that field line may not be able to observe any precipitation when the EMIC waves are intense, and ironically may only observe non-resonantly interacting electrons at a few 100 keV energies, that are below the minimum resonant energy (Capannolo et al., 2018, 2019; Chen et al., 2016; Hendry et al., 2017; Usanova et al., 2014). Indeed a recent observation showing a negative slope of the pitch angle distribution at low pitch angles following EMIC scattering in Van Allen Probes data support the nonlinear precipitation blocking effect (Zhu et al., 2020).

It should also be noted that the force bunching effect is typically omitted in the estimation of nonlinear effects. For example, the standard, traditionally used "inhomogeneity parameter" R, provides a measure of the competition between wave-driven effects compared to the inhomogeneity of the background magnetic field and can be written as (eq. (7) in Albert & Bortnik, 2009):

$$R \approx -\frac{9\lambda}{2L}\frac{mc}{eB_w}\frac{c}{R_E}\frac{p}{mc}\frac{\cos^2\alpha}{\sin\alpha}\frac{1}{1-\omega/\Omega_i} \tag{5}$$
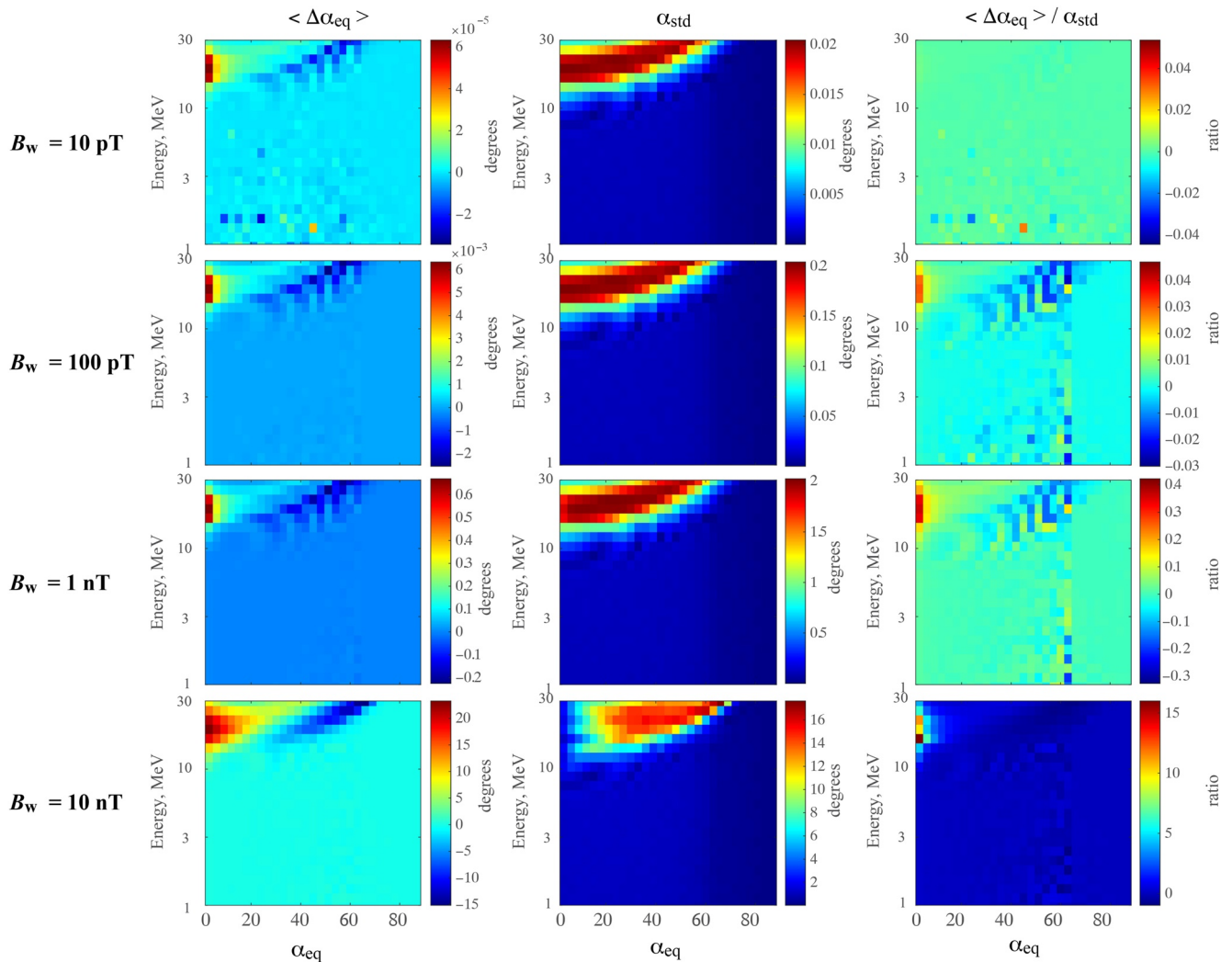
Figure 4. Scattering characteristics corresponding to Region (b) Similar format to Figure 3, but for the low-density region outside the plasmapause, with scattering driven by H-band EMIC waves. Note the changing color scales in each panel.

for a dipolar background magnetic field, and a small latitude approximation. Here $|R| \gg 1$ indicates linear behavior, whereas $|R| \ll 1$ points to essentially nonlinear particle motion. In the case of interaction near the minimum resonant energy, $\alpha \to 0$ suggests that $|R| \to \infty$ (which can also be seen in Figure 1 of Albert and Bortnik (2009)) indicating that predominantly linear behavior is expected at such low pitch angles (though more recent work has started to incorporate the force bunching effect, e.g., quantities R2, R3 and δ of Albert et al. (2021)).

At larger pitch angles, when particle energies are close to the resonant energy, the conventional nonlinear "phase bunching" effect begins to dominate the advective motion of the energetic electrons in pitch angle, and acts in the same direction as force bunching (dominant at low pitch angles), namely acting to rapidly transport the mean pitch angle to larger values. The signature of this phase bunching effect can be seen as the positive advection (red) band in Figure 3 (left column, at pitch angles immediately below the "phase trapping" blue band) and has been understood and described in previous studies (e.g., Albert & Bortnik, 2009; Grach & Demekhov, 2018a, 2018b, 2020; Kubota & Omura, 2017). Near the minimum resonant energy, the phase bunching effect takes place at low pitch angles and approaches the force bunching effect, creating a combined effect that rapidly transports low pitch angle particles to much larger pitch angles.

The forgoing analysis has been performed for a monochromatic EMIC wave, both for simplicity, and indeed as it represents wave packets that are narrowband or whose frequency is slowly varying. However, it is important

to note that for EMIC wave packets whose amplitude is rapidly varying, or that have a wide frequency band, additional effects may enter that disrupt (or sometimes enhance) the nonlinear effects described in this study (e.g., Grach et al., 2021). Additionally, we note that although force bunching has been demonstrated to be very effective, the final flux of precipitating electrons within the loss-cone will be determined by a delicate balance between electrons at large pitch angles transported directly into the loss-cone (due to phase trapping) and low pitch-angle electrons transported away from the loss-cone by force bunching. This balance depends on the EMIC wave amplitude, that is, when the advection term becomes comparable to the initial pitch angle (e.g., left column of Figure 3, noting that $\Delta\alpha_{eq}$ becomes comparable to α_{eq} at $B_w \sim 10$ nT) as well as the background plasma characteristics, and shall be investigated both observationally (using case studies of observed electron precipitation) and theoretically in future studies.

In summary, the term "precipitation blocking" refers to the ability of the force bunching nonlinear effect (combined with the phase bunching effect near the minimum resonant energy) to potentially prevent the electron precipitation expected on the basis of quasilinear theory and the conventional nonlinear theory (e.g., Equation 5) which often omits the second (force bunching) term in the wave particle phase Equation 3.

5. Summary and Conclusions

Using nonlinear test-particle simulations, we have characterized the behavior of energetic electrons interacting with different groups of EMIC waves, that have been recently identified using Van Allen Probes and Arase data (Jun et al., 2021). Two different wave populations were chosen due to their occurrence at low L-shells and overlap with the high flux portion of the outer radiation belt electrons: region b waves that are characterized by H-band EMIC waves and occur in the low density, dayside region outside the plasmasphere, and region c waves that are predominantly He-band EMIC waves, and occur in the high-density, duskside region within the plasmasphere (and duskside bulge region). We find that:

1. Both groups of EMIC waves can drive a variety of wave-particle interactions including: diffusive (quasilinear) scattering, phase trapping (advection to low pitch angles), phase bunching (advection to large pitch angles), and force bunching which results in rapid advection of low pitch angle particles to larger pitch angles.
2. Region b (low density, H-band) EMIC waves show similar qualitative behavior to region c waves, but have minimum resonant energies in excess of 16 MeV, which makes this population relatively ineffective for scattering the bulk of the ~MeV outer radiation belt electrons.
3. The effects of nonlinear force bunching at low pitch angles, especially in combination with phase bunching near the minimum resonant energy, can result in "precipitation blocking" due to the rapid advection of particles out of the loss cone and toward much larger pitch angles where the particles are stably trapped.
4. Increasing EMIC wave amplitudes cause the positive advection due to force bunching to dominate over diffusive scattering above $B_w \sim 200$ pT. As a result, the larger the EMIC wave amplitude, the more the electron precipitation at, and above the minimum resonant energy should be blocked.

The results presented in this study are applicable to a single-pass interaction of electrons streaming through the EMIC wave packet, and could have profound implications for observational conjunction studies. For example, studies that aim to observe the direct electron precipitation on spacecraft located at Low Earth Orbit, driven by an EMIC wave packet observed by a second, in situ spacecraft located near the geomagnetic equator. The effects of EMIC wave intensity upon the longer-term, multi-pass interaction (when competing nonlinear effects have had an opportunity to compensate for each other), and in particular the expected precipitation signature, remains to be fully investigated.

Conflict of Interest

The authors declare no conflicts of interest relevant to this study.

Data Availability Statement

The results obtained in the present paper rely on the MATLAB programming language (https://www.mathworks.com/), and an integration of the set of differential Equations 1–4 presented in Section 2 of the paper, using the ode113 built-in numerical function. No new data was used in this paper.

References

Albert, J. M. (2003). Evaluation of quasi-linear diffusion coefficients for EMIC waves in a multispecies plasma. *Journal of Geophysical Research*, *108*(A6), 1249. https://doi.org/10.1029/2002JA009792

Albert, J. M., Artemyev, A. V., Li, W., Gan, L., & Ma, Q. (2021). Models of resonant wave-particle interactions. *Journal of Geophysical Research: Space Physics*, *126*, e2021JA029216. https://doi.org/10.1029/2021ja029216

Albert, J. M., & Bortnik, J. (2009). Nonlinear interaction of radiation belt electrons with electromagnetic ion cyclotron waves. *Geophysical Research Letters*, *36*, L12110. https://doi.org/10.1029/2009gl038904

Anderson, B. J., Denton, R. E., Ho, G., Hamilton, D. C., Fuselier, S. A., & Strangeway, R. J. (1996). Observational test of local proton cyclotron instability in the Earth's magnetosphere. *Journal of Geophysical Research*, *101*, 527–21543. https://doi.org/10.1029/96JA01251

Anderson, B. J., Erlandson, R. E., & Zanetti, L. J. (1992a). A statistical study of Pc 1–2 magnetic pulsations in the equatorial magnetosphere: I. Equatorial occurrence distributions. *Journal of Geophysical Research*, *97*, 3075–3088. https://doi.org/10.1029/91JA02706

Anderson, B. J., Erlandson, R. E., & Zanetti, L. J. (1992b). A statistical study of Pc 1–2 magnetic pulsations in the equatorial magnetosphere. II—wave properties. *Journal of Geophysical Research*, *97*, 3089–3101. https://doi.org/10.1029/91JA02706

Artemyev, A. V., Neishtadt, A. I., Albert, J. M., Gan, L., Li, W., & Ma, Q. (2021). Theoretical model of the nonlinear resonant interaction of whistler-mode waves and field aligned electrons. *Physics of Plasmas*, *28*, 052902. https://doi.org/10.1063/5.0046635

Bortnik, J., Inan, U. S., & Bell, T. F. (2006). Temporal signatures of radiation belt electron precipitation induced by lightning-generated MR whistler waves: 1. Methodology. *Journal of Geophysical Research*, *111*, A02204. https://doi.org/10.1029/2005JA011182

Bortnik, J., & Thorne, R. M. (2010). Transit time scattering of energetic electrons due to equatorially confined magnetosonic waves. *Journal of Geophysical Research*, *115*, A07213. https://doi.org/10.1029/2010JA015283

Bortnik, J., Thorne, R. M., & Inan, U. S. (2008). Nonlinear interaction of energetic electrons with large amplitude chorus. *Geophysical Research Letters*, *35*, L21102. https://doi.org/10.1029/2008gl035500

Capannolo, L., Li, W., Ma, Q., Chen, L., Shen, X.-C., Spence, H. E., et al. (2019). Direct observation of subrelativistic electron precipitation potentially driven by EMIC waves. *Geophysical Research Letters*, *46*. https://doi.org/10.1029/2019gl084202

Capannolo, L., Li, W., Ma, Q., Zhang, X.-J., Redmon, R. J., Rodriguez, J. V., et al. (2018). Understanding the driver of energetic electron precipitation using coordinated multisatellite measurements. *Geophysical Research Letters*, *45*, 6755–6765. https://doi.org/10.1029/2018GL078604

Carpenter, D. L., & Anderson, R. R. (1992). An ISEE/whistler model of equatorial electron density in the magnetosphere. *Journal of Geophysical Research*, *97*, 1097. https://doi.org/10.1029/91ja01548

Chen, L., Thorne, R. M., Bortnik, J., & Zhang, X.-J. (2016). Nonresonant interactions of electromagnetic ion cyclotron waves with relativistic electrons. *Journal of Geophysical Research: Space Physics*, *121*, 9913–9925. https://doi.org/10.1002/2016JA022813

Denton, R. E., Goldstein, J., & Menietti, J. D. (2002). Field line dependence of magnetospheric electron density. *Geophysical Research Letters*, *29*(24), 2205–2211. https://doi.org/10.1029/2002GL015963

Engebretson, M. J., Posch, J. L., Wygant, J. R., Kletzing, C. A., Lessard, M. R., Huang, C. L., et al. (2015). Van Allen probes, NOAA, GOES, and ground observations of an intense EMIC wave event extending over 12 h in magnetic local time. *Journal of Geophysical Research: Space Physics*, *120*, 5465–5488. https://doi.org/10.1002/2015ja021227

Fraser, B. J., Grew, R. S., Morley, S. K., Green, J. C., Singer, H. J., Loto'aniu, T. M., & Thomsen, M. F. (2010). Storm time observations of electromagnetic ion cyclotron waves at geosynchronous orbit: GOES results. *Journal of Geophysical Research*, *115*, A05208. https://doi.org/10.1029/2009JA014516

Gomberoff, L., & Neira, R. (1983). Convective growth rate of ion cyclotron waves in a H^+-He^+ and H^+-He^+-O^+ plasma. *Journal of Geophysical Research*, *88*, 2170–2174. https://doi.org/10.1029/ja088ia03p02170

Grach, V. S., & Demekhov, A. G. (2018a). Resonance interaction of relativistic electrons with ion-cyclotron waves. I. Specific features of the nonlinear interaction regimes. *Radiophysics and Quantum Electronics*, *60*(12), 942–959. https://doi.org/10.1007/s11141-018-9860-0

Grach, V. S., & Demekhov, A. G. (2018b). Resonant interaction of relativistic electrons with electromagnetic ion–cyclotron waves. II. Integral parameters of interaction regimes. *Radiophysics and Quantum Electronics*, *61*(6), 389–401. https://doi.org/10.1007/s11141-018-9900-9

Grach, V. S., & Demekhov, A. G. (2020). Precipitation of relativistic electrons under resonant interaction with electromagnetic ion cyclotron wave packets. *Journal of Geophysical Research: Space Physics*, *125*, e2019JA027358. https://doi.org/10.1029/2019ja027358

Grach, V. S., Demekhov, A. G., & Larchenko, A. V. (2021). Resonant interaction of relativistic electrons with realistic electromagnetic ion–cyclotron wave packets. *Earth Planets and Space*, *73*, 129. https://doi.org/10.1186/s40623-021-01453-w

Halford, A. J., Fraser, B. J., & Morley, S. K. (2010). EMIC wave activity during geomagnetic storm and nonstorm periods: CRRES results. *Journal of Geophysical Research*, *115*, A12248. https://doi.org/10.1029/2010JA015716

Hendry, A. T., Rodger, C. J., & Clilverd, M. A. (2017). Evidence of sub-MeV EMIC-driven electron precipitation. *Geophysical Research Letters*, *44*(3), 1210–1218. https://doi.org/10.1002/2016gl071807

Horne, R. B., & Thorne, R. (1994). Convective instabilities of electromagnetic ion cyclotron waves in the outer magnetosphere. *Journal of Geophysical Research*, *99*(A9), 17259–17273. https://doi.org/10.1029/94ja01259

Horne, R. B., & Thorne, R. M. (1993). On the preferred source location for the convective amplification of ion cyclotron waves. *Journal of Geophysical Research*, *98*, 9233–9247. https://doi.org/10.1029/92JA02972

Inan, U. S., Bell, T. F., & Helliwell, R. A. (1978). Nonlinear pitch angle scattering of energetic electrons by coherent VLF waves in the magnetosphere. *Journal of Geophysical Research*, *83*, 3235–3253. https://doi.org/10.1029/ja083ia07p03235

Jordanova, V. K., Albert, J., & Miyoshi, Y. (2008). Relativistic electron precipitation by EMIC waves from self-consistent global simulations. *Journal of Geophysical Research*, *113*, A00A10. https://doi.org/10.1029/2008JA013239

Jordanova, V. K., Miyoshi, Y. S., Zaharia, S., Thomsen, M. F., Reeves, G. D., Evans, D. S., et al. (2006). Kinetic simulations of ring current evolution during the Geospace Environment Modeling challenge events. *Journal of Geophysical Research*, *111*, A11S10. https://doi.org/10.1029/2006JA011644

Jun, C.-W., Miyoshi, Y., Kurita, S., Yue, C., Bortnik, J., Lyons, L., et al. (2021). The characteristics of EMIC waves in the magnetosphere based on the Van Allen Probes and Arase observations. *Journal of Geophysical Research: Space Physics*, *126*, e2020JA029001. https://doi.org/10.1029/2020ja029001

Kasahara, Y., Sawada, A., Yamamoto, M., Kimura, I., Kokubun, S., & Hayashi, K. (1992). Ion cyclotron emissions observed by the satellite Akebono in the vicinity of the magnetic equator. *Radio Science*, *27*(2), 347–362. https://doi.org/10.1029/91RS01872

Keika, K., Takahashi, K., Ukhorskiy, A. Y., & Miyoshi, Y. (2013). Global characteristics of electromagnetic ion cyclotron waves: Occurrence rate and its storm dependence. *Journal of Geophysics Research Space Physics*, *118*, 4135–4150. https://doi.org/10.1002/jgra.50385

Kennel, C. F., & Petschek, H. E. (1966). Limits on stably trapped particle fluxes. *Journal of Geophysical Research*, *71*, 1–28. https://doi.org/10.1029/jz071i001p00001

Kitahara, M., & Katoh, Y. (2019). Anomalous trapping of low pitch angle electrons by coherent whistler mode waves. *Journal of Geophysical Research: Space Physics*, *124*, 5568–5583. https://doi.org/10.1029/2019ja026493

Kozyra, J. U., Cravens, T. E., Nagy, A. F., Fontheim, E. G., & Ong, R. S. B. (1984). Effects of energetic heavy ions on electromagnetic ion cyclotron wave generation in the plasmapause region. *Journal of Geophysical Research*, *89*, 2217–2233. https://doi.org/10.1029/JA089iA04p02217

Kubota, Y., & Omura, Y. (2017). Rapid precipitation of radiation belt electrons induced by emic rising tone emissions localized in longitude inside and outside the plasmapause. *Journal of Geophysical Research: Space Physics*, *122*, 293–309. https://doi.org/10.1002/2016ja023267

Li, W., & Hudson, M. K. (2019). Earth's van allen radiation belts: From discovery to the van allen probes era. *Journal of Geophysical Research: Space Physics*, *124*. https://doi.org/10.1029/2018ja025940

Liu, K., Winske, D., Gary, S. P., & Reeves, G. D. (2012). Relativistic electron scattering by large amplitude electromagnetic ion cyclotron waves: The role of phase bunching and trapping. *Journal of Geophysical Research*, *117*, A06218. https://doi.org/10.1029/2011JA017476

Loto'aniu, T. M., Fraser, B. J., & Waters, C. L. (2005). Propagation of electromagnetic ion cyclotron wave energy in the magnetosphere. *Journal of Geophysical Research*, *110*, A07214. https://doi.org/10.1029/2004JA010816

Lundin, B. V., & Shklyar, D. R. (1977). Interaction of electrons with low transverse velocities with VLF waves in an inhomogeneous plasma. *Geomagnetism and Aeronomy*, *17*(2), 246–251.

Mauk, B. H., Fox, N. J., Kanekal, S. G., Kessel, R. L., Sibeck, D. G., & Ukhorskiy, A. (2013). Science objectives and rationale for the radiation belt storm probes mission. *Space Science Reviews*, *179*, 3–27. https://doi.org/10.1007/s11214-012-9908-y

Mauk, B. H., & Mcpherron, R. L. (1980). An experimental test of the electromagnetic ion cyclotron instability within the Earth's magnetosphere. *Physics of Fluids*, *23*, 2111–2127. https://doi.org/10.1063/1.862873

Meredith, N. P., Horne, R. B., Kersten, T., Fraser, B. J., & Grew, R. S. (2014). Global morphology and spectral properties of EMIC waves derived from CRRES observations. *Journal of Geophysical Research: Space Physics*, *119*, 5328–5342. https://doi.org/10.1002/2014JA020064

Meredith, N. P., Thorne, R. M., Horne, R. B., Summers, D., Fraser, B. J., & Anderson, R. R. (2003). Statistical analysis of relativistic electron energies for cyclotron resonance with EMIC waves observed on CRRES. *Journal of Geophysical Research*, *108*(A6), 1250. https://doi.org/10.1029/2002JA009700

Min, K., Lee, J., Keika, K., & Li, W. (2012). Global distribution of EMIC waves derived from THEMIS observations. *Journal of Geophysical Research*, *117*, A05219. https://doi.org/10.1029/2012JA017515

Miyoshi, Y., Sakaguchi, K., Shiokawa, K., Evans, D., Albert, J., Connors, M., & Jordanova, V. (2008). Precipitation of radiation belt electrons by EMIC waves, observed from ground and space. *Geophysics Research Letters*, *35*, L23101. https://doi.org/10.1029/2008GL035727

Miyoshi, Y., Shinohara, I., Takashima, T., Asamura, K., Higashio, N., Mitani, T., et al. (2018). Geospace exploration project ERG. *Earth Planets and Space*, *70*, 101. https://doi.org/10.1186/s40623-018-0862-0

Omura, Y., & Zhao, Q. (2012). Nonlinear pitch angle scattering of relativistic electrons by EMIC waves in the inner magnetosphere. *Journal of Geophysical Research*, *117*, A08227. https://doi.org/10.1029/2012JA017943

Omura, Y., & Zhao, Q. (2013). Relativistic electron microbursts due to nonlinear pitch angle scattering by EMIC triggered emissions. *Journal of Geophysical Research: Space Physics*, *118*, 5008–5020. https://doi.org/10.1002/jgra.50477

Rae, I. J., Murphy, K. R., Watt, C. E. J., Sandhu, J. K., Georgiou, M., Degeling, A. W., et al. (2019). How do ultra-low frequency waves access the inner magnetosphere during geomagnetic storms? *Geophysical Research Letters*, *46*, 10699–10709. https://doi.org/10.1029/2019GL082395

Rauch, J. L., & Roux, A. (1982). Ray tracing of ULF waves in a multicomponent magnetospheric plasma: Consequences for the generation mechanism of ion cyclotron waves. *Journal of Geophysical Research*, *87*(10), 8191–8198. https://doi.org/10.1029/JA087iA10p08191

Saikin, A. A., Zhang, J.-C., Allen, R. C., Smith, C. W., Kistler, L. M., Spence, H. E., et al. (2015). The occurrence and wave properties of H^+-, He^+-, and O^+-band EMIC waves observed by the Van Allen Probes. *Journal of Geophysical Research: Space Physics*, *120*, 7477–7492. https://doi.org/10.1002/2015ja021358

Shprits, Y. Y., Chen, L., & Thorne, R. M. (2009). Simulations of pitch angle scattering of relativistic electrons with MLT-dependent diffusion coefficients. *Journal of Geophysical Research*, *114*, A03219. https://doi.org/10.1029/2008JA013695

Shprits, Y. Y., Drozdov, A. Y., Spasojevic, M., Kellerman, A. C., Usanova, M. E., Engebretson, M. J., et al. (2016). Wave-induced loss of ultra-relativistic electrons in the Van Allen radiation belts. *Nature Communications*, *7*(1), 12883. https://doi.org/10.1038/ncomms12883

Shprits, Y. Y., Kellerman, A., Aseev, N., Drozdov, A. Y., & Michaelis, I. (2017). Multi-MeV electron loss in the heart of the radiation belts. *Geophysical Research Letters*, *44*, 1204–1209. https://doi.org/10.1002/2016GL072258

Summers, D., & Thorne, R. M. (2003). Relativistic electron pitch-angle scattering by electromagnetic ion cyclotron waves during geomagnetic storms. *Journal of Geophysical Research*, *108*(A4), 1143. https://doi.org/10.1029/2002JA009489

Thorne, R. M., Horne, R. B., Glauert, S. A., Meredith, N. P., Shprits, Y. Y., Summers, D., & Anderson, R. R. (2005). Dynamic evolution of energetic outer zone electrons due to wave-particle interactions during storms. In J. L. Burch, M. Schulz, & H. Spence (Eds.) (Vol. 159, pp. 101–112). AGU. *Inner magnetosphere interactions: New perspectives from imaging, geophysics monograph series*. https://doi.org/10.1029/159gm07

Thorne, R. M., Horne, R. B., Jordanova, V. K., Bortnik, J., & Glauert, S. A. (2006). Interaction of EMIC waves with thermal plasma and radiation belt particles. In J. L. Burch, M. Schulz, & H. Spence, (Eds.) (Vol. 169, pp. 213–223). AGU. *Magnetospheric ULF waves: Synthesis and new directions, geophysical monograph series*. https://doi.org/10.1029/169gm14

Thorne, R. M., & Kennel, C. F. (1971). Relativistic electron precipitation during magnetic storm main phase. *Journal of Geophysical Research*, *76*(19), 4446–4453. https://doi.org/10.1029/JA076i019p04446

Usanova, M. E., Darrouzet, F., Mann, I. R., & Bortnik, J. (2013). Statistical analysis of EMIC waves in plasmaspheric plumes from Cluster observations. *Journal of Geophysical Research: Space Physics*, *118*, 4946–4951. https://doi.org/10.1002/jgra.50464

Usanova, M. E., Drozdov, A., Orlova, K., Mann, I. R., Shprits, Y., Robertson, M. T., et al. (2014). Effect of EMIC waves on relativistic and ultrarelativistic electron populations: Ground-based and Van Allen Probes observations. *Geophysical Research Letters*, *41*, 1375–1381. https://doi.org/10.1002/2013gl059024

Usanova, M. E., Mann, I. R., Bortnik, J., Shao, L., & Angelopoulos, V. (2012). THEMIS observations of electromagnetic ion cyclotron wave occurrence: Dependence on AE, SYMH, and solar wind dynamic pressure. *Journal of Geophysical Research*, *117*, A10218. https://doi.org/10.1029/2012JA018049

Walker, A. D. M. (1993). *Plasma waves in the magnetosphere*. Springer-Verlag.

Young, D. T., Perraut, S., Roux, A., De Villedary, C., Gendrin, R., Korth, A., et al. (1981). Wave-particle interactions near $\Omega_{He}+$ observed on GEOS 1 and 2: 1. Propagation of ion cyclotron waves in He$^+$-rich plasma. *Journal of Geophysical Research*, *86*, 6755–6772. https://doi.org/10.1029/JA086iA08p06755

Zheng, L., Chen, L., & Zhu, H. (2019). Modeling energetic electron nonlinear wave-particle interactions with electromagnetic ion cyclotron waves. *Journal of Geophysical Research: Space Physics*, *124*, 3436–3453. https://doi.org/10.1029/2018ja026156

Zhu, H., Chen, L., Claudepierre, S. G., & Zheng, L. (2020). Direct evidence of the pitch angle scattering of relativistic electrons induced by EMIC waves. *Geophysical Research Letters*, *47*, e2019GL085637. https://doi.org/10.1029/2019GL085637